Block Copolymers—Designer Soft Materials

Advances in synthetic chemistry and statistical theory provide unparalleled control over molecular scale morphology in this class of macromolecules.

Frank S. Bates and Glenn H. Fredrickson

Block copolymers are all around us, found in such products as upholstery foam, adhesive tape and asphalt additives. This class of macromolecules is produced by joining two or more chemically distinct polymer blocks, each a linear series of identical monomers, that may be thermodynamically incompatible (like oil and vinegar). Segregation of these blocks on the molecular scale (5–100 nm) can produce astonishingly complex nanostructures, such as the "knitting pattern" shown on the cover of this issue of PHYSICS TODAY. This striking pattern, discovered by Reimund Stadler and his coworkers,[1] reflects a delicate free-energy minimization that is common to all block copolymer materials.

All block copolymers belong to a broad category of condensed matter sometimes referred to collectively as soft materials, which, in contrast to crystalline solids, are characterized by fluidlike disorder on the molecular scale and a high degree of order at longer length scales. Their complex structure can give block copolymers many useful and desirable properties. The familiar polyurethane foams used in upholstery and bedding are composed of multiblock copolymers known as thermoplastic elastomers that combine high-temperature resilience and low-temperature flexibility. Common, inexpensive box tape employs a different type of block copolymer, a linear triblock, to achieve pressure-sensitive adhesion. The addition of appropriate block copolymers to commodity plastics such as polystyrene can enhance toughness, or modify the surface properties for applications as diverse as colloidal stabilization, medical implantation and microelectronic fabrication. In certain regions of the world, particularly in Europe, block copolymers are blended with asphalt to reduce pavement cracking and rutting at low and high temperature extremes, respectively.

Two decades of theoretical development have culminated in remarkably predictive statistical theories that can account for the domain shapes, dimensions, connectivity and ordered symmetry of many types of block copolymers. Now, recent advances in synthetic chemistry have exposed fresh opportunities for using judicious combinations of multiple blocks in novel molecular architectures to produce a seemingly unlimited number of exquisitely structured materials endowed with tailored mechanical, optical, electrical, ionic, barrier and other physical properties. This article summarizes the current understanding of block copolymer morphology. (If you want to learn more about block copolymers, reference 2 is a good place to start; there you will also find additional references for much of the work described in this article.)

FRANK S. BATES *is a Distinguished McKnight University Professor of Chemical Engineering and Materials Science at the University of Minnesota in Minneapolis.* GLENN H. FREDRICKSON *is a professor in, and chair of, the chemical engineering department at the University of California, Santa Barbara.*

Building blocks

A stunning array of block configurations can be constructed using modern synthetic chemistry techniques. Figure 1 illustrates a basic classification of these molecular architectures, based on two parameters: (1) the number of chemically distinct blocks, and (2) linear versus branched sequencing of the blocks. Obviously, figure 1 depicts a limited collection of the enormous range of molecular architectures. Nevertheless, essentially all known morphologies can be understood based on the principles developed using these examples.

The simplest and most studied architecture is the linear AB diblock, consisting of a long sequence of type A monomers covalently bonded to a chain of type B monomers. ABA triblocks and $(AB)_n$ multiblocks are formed by coupling additional A and B blocks. Use of three or more monomer types during polymer synthesis leads to the formation of ABC or other multicomponent molecular architectures. (The knitting pattern on the cover is a linear ABC triblock). Various chemical coupling strategies permit the polymer chemist to configure two, three or more polymer molecules into branched architectures as illustrated in figure 1. Subtle variations in the molecular topology—for example ABC versus ACB, or star-ABC (where blocks are not linear but are joined in the center)—can lead to pronounced changes in morphology, as well as material properties, as discussed below.

Although innovative developments in polymer chemistry have catalyzed the creation of many useful types of block copolymers, practical difficulties in copolymer synthesis remain. In most chemical synthesis reactions, normal chemical kinetics results in a distribution of molecular weights, and in block copolymers this results in compositional heterogeneity. Nevertheless, most model polymers can be prepared with relatively narrow block molecular weight distributions. For the remainder of this article, we assume ideal (monodisperse and compositionally uniform) molecular architectures when discussing block co-

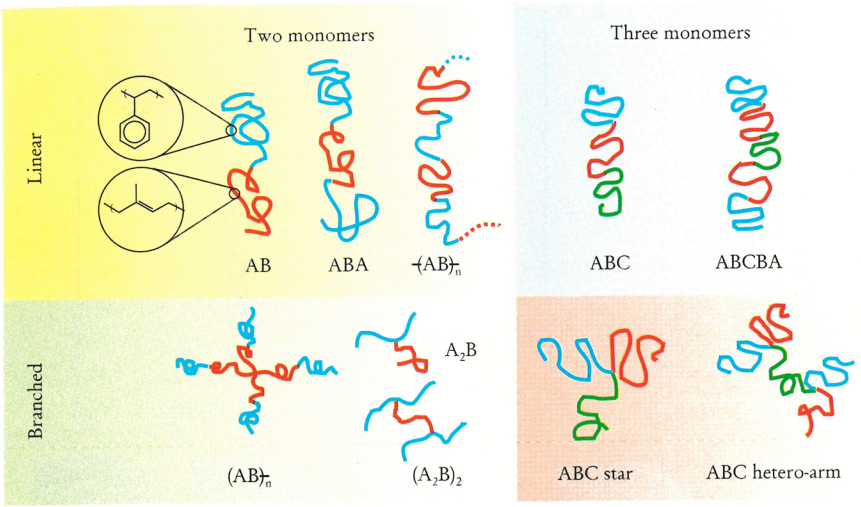

FIGURE 1. BLOCK COPOLYMERS can be configured into a nearly limitless number of molecular architectures based on two, three or more monomer types. Here, architectures are classified by number of monomer types and topology (linear versus branched sequencing). Each colored strand represents a polymer block composed of a linear sequence of same-type monomers, with monomer types A, B and C shown as blue, red and green, respectively. The colored strands are joined as shown to form the block copolymer macromolecule. The upper-left inset shows two representative monomer chemical structures, with the diameter of the circle showing the typical monomer length scale a.

polymer phase behavior. However, many commercially relevant block copolymers are characterized by considerable block molecular weight heterogeneity that can distort or even preclude altogether the phenomena we describe here.

Physics of microphase separation

The unique properties, and so the applications, of block copolymer materials rely crucially on their mesoscopic (10 nm scale) self-assembly in the molten and solid states. As illustrated by the knitting pattern on the cover, this collective self-assembly produces spatially periodic composition patterns that can exhibit considerable complexity. These patterns are commonly referred to as microphases, mesophases or nanophases, depending on length scale; here, we consistently adopt the historical term "microphase separation" to describe the formation of patterns in block copolymer melts.

Microphase separation is driven by chemical incompatibilities between the different blocks that make up block copolymer molecules. In the simplest case of a diblock copolymer (as on the left side of figure 1), there is only the issue of compatibility between the dissimilar A and B blocks. Unlike binary mixtures of low molecular weight fluids, the entropy of mixing per unit volume of dissimilar polymers is small (varying inversely with molecular weight). Thus, even minor chemical or structural differences between A and B blocks are sufficient to produce excess free-energy contributions that are usually unfavorable to mixing. As an extreme example, even polymer isotopes, such as polystyrene and deuterated-polystyrene, have been demonstrated to be immiscible at sufficiently high molecular weight. The nonideal part of the mixing free energy is commonly described in terms of a "Flory–Huggins interaction parameter,"

$$\chi_{AB} = (Z/k_BT)[\varepsilon_{AB} - (\tfrac{1}{2})(\varepsilon_{AA} + \varepsilon_{BB})],$$

which describes the free-energy cost per monomer (in units of the thermal energy k_BT) of contacts between A and B monomers. In this definition, Z is the number of nearest-neighbor monomers to a copolymer configuration cell, and ε_{AB} is the interaction energy per monomer between A and B monomers. Positive χ_{AB} indicates net repulsion between species A and B, whereas a negative value indicates a free-energy drive towards mixing. For typical

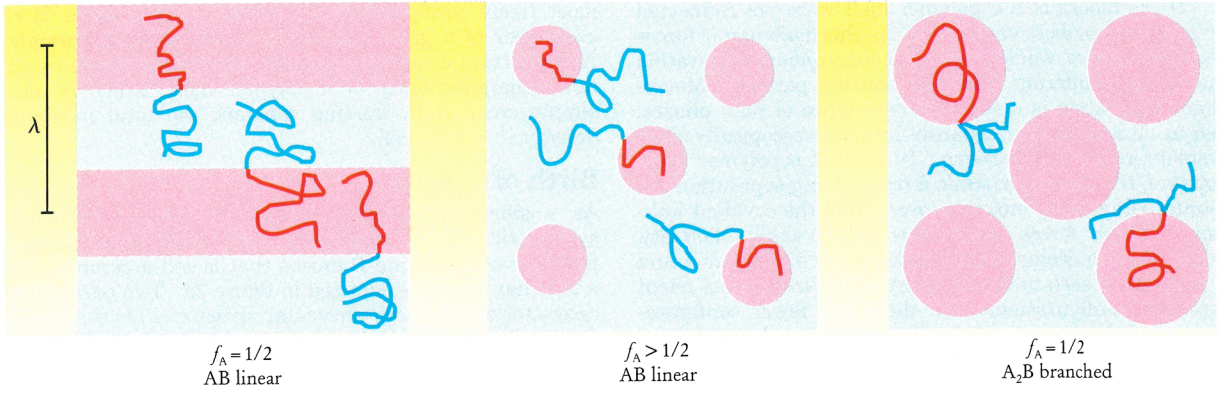

FIGURE 2. DIBLOCK MORPHOLOGY depends on block composition. Interfacial curvature of block copolymers can be controlled by adjusting the composition f or changing the molecular architecture. Shaded regions are block-segregated microdomains colored according to monomer type, with blue for type A and red for type B monomers. **a:** Self-assembly of symmetric ($f_A = f_B = 1/2$) linear AB diblocks leads to a lamellar morphology. **b:** Increasing the volume fraction of one block (in this case, $f_A > 1/2$) induces interfacial curvature, resulting in a nonlamellar morphology, such as cylindrical or spherical. **c:** A branched A_2B architecture can result in a nonlamellar morphology even in a compositionally symmetric molecule, due to asymmetric interfacial crowding.

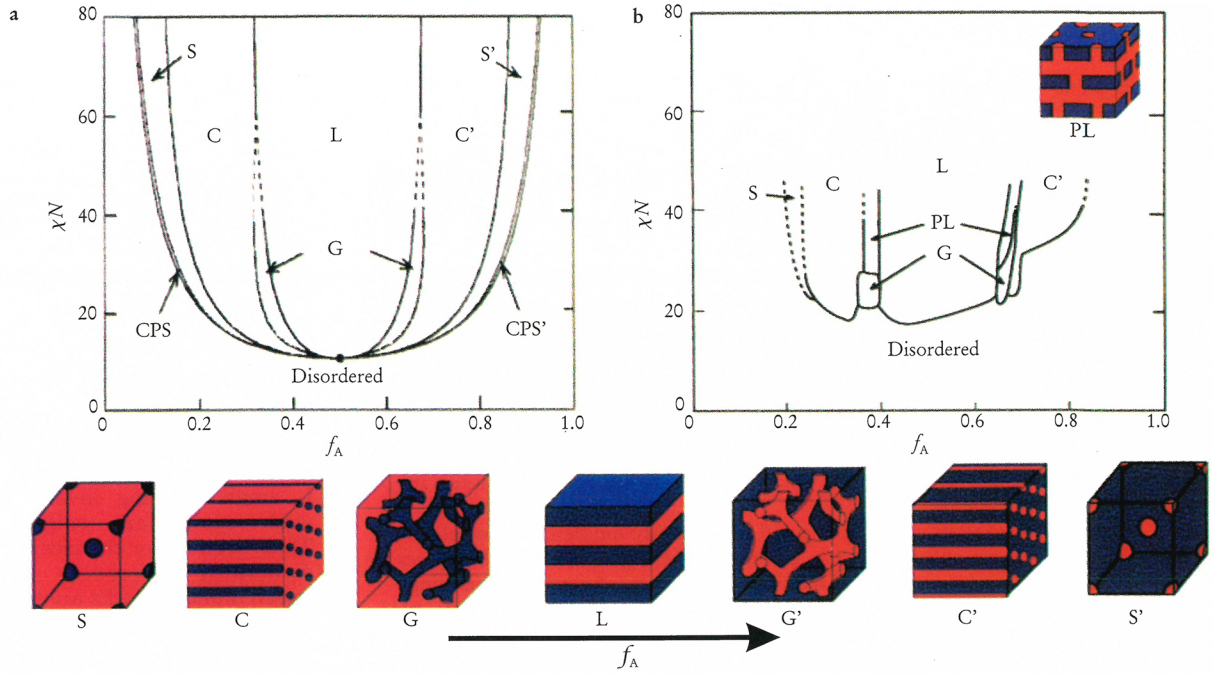

FIGURE 3. PHASE DIAGRAM for linear AB diblock copolymers, comparing theory and experiment. **a:** Self-consistent mean-field theory[8] predicts four equilibrium morphologies: spherical (S), cylindrical (C), gyroid (G) and lamellar (L), depending on the composition f and combination parameter χN. Here, χ is the segment–segment interaction energy (proportional to the heat of mixing A and B segments) and N is the degree of polymerization (number of monomers of all types per macromolecule). **b:** Experimental phase portrait for poly(isoprene-styrene) diblock copolymers.[9] The resemblance to the theoretical diagram is remarkable, though there are important differences, as discussed in the text. One difference is the observed PL phase, which is actually metastable. Shown at the bottom of the figure is a representation of the equilibrium microdomain structures as f_A is increased for fixed χN, with type A and B monomers confined to blue and red regions, respectively.

dissimilar monomer pairs in which there are no strong specific interactions (hydrogen bonding, charges or the like), χ_{AB} is positive and small compared with unity (for example, χ_{SI} between styrene and isoprene is of order 0.1). Moreover, χ_{AB} usually varies inversely with temperature, so that mixing is promoted as the temperature rises. Virtually all modern theories of microphase separation employ this simple one-parameter thermodynamic description of the driving force for microphase separation.

If the blocks of a copolymer melt were not connected by covalent bonds to each other, the thermodynamic forces described above would lead to a *macrophase* separation that is very different from the knitting pattern. Macrophase separation is a state of coexistence of bulk phases, just as oil and vinegar separate into macroscopically sized droplets in a salad dressing. In a block copolymer melt, however, the thermodynamic forces driving separation are counterbalanced by entropic forces from the covalent linkages. These forces, sometimes called chain elasticity, reflect the requirement that, to keep the dissimilar A and B portions of each molecule apart, copolymers must adopt extended configurations. As there are fewer configurations available to extended polymer chains than to those in their native randomly coiled state, an entropic restoring force is generated that serves to limit the phase separation between A and B blocks to mesoscopic dimensions. The entropic force law is approximately Hookian, and provides the basis for understanding the elasticity of rubberlike materials. For a chain or block of N monomers extended to a distance R, the elastic free energy that leads to the entropic force can be expressed as $F_e = 3k_BTR^2/(2Na^2)$, where a is a monomer size scale that depends on the local structure of the polymer chain (roughly the diameter of either of the magnified circles shown in the AB configuration of figure 1).

The primary challenge for theories of microphase separation is to accurately sum the competing free-energy contributions of interaction energy and elastic energy within the unit cell of a periodic microphase structure. Minimization of the free energy for a particular geometry (compared to all other candidate geometries) indicates the most likely configuration and scale lengths for a block copolymer of a given composition and molecular weight. An important constraint in such calculations is the essential incompressibility of a polymer melt, which is most simply ensured by holding constant the total monomer density in a unit cell.

Birth of a phase

As a simple illustration of such a theory, consider a symmetric diblock copolymer melt with equal volume fractions of the A and B blocks that is self-assembled into a lamellar phase as depicted in figure 2a. Two parameters characterize the block molecular structure: (1) the overall degree of polymerization N, which is the total number of monomers per macromolecule, and (2) the composition $f_A = N_A/N$, where N_A is the number of A monomers per molecule. For the symmetric diblock, $f_A = f_B = 1/2$.

At low temperatures (large χ_{AB}), the segregation is strong, leading to microdomains that are nearly pure in A and B, separated by interfaces that are much narrower than the lamellar domain period λ. By further assuming that the chains are all uniformly stretched, we can write the following expression for the sum of the interaction

and elastic energies per copolymer chain of a lamellar phase:

$$F_{lamellar}/k_BT = 3(\lambda/2)^2/(2Na^2) + (\gamma_{AB}/k_BT)\Sigma. \quad (1)$$

The first term is the stretching energy for a chain of N total monomers to extend a half-period in the lamellar phase. The second term describes interactions that are confined to the narrow interfacial regions between A and B microdomains. This interaction energy per copolymer chain is expressed as a product of the A–B interfacial tension, γ_{AB}, and the interfacial area per chain, Σ. According to a classical theory of polymer–polymer interfaces, $\gamma_{AB} = (k_BT/a^2)\sqrt{\chi_{AB}/6}$. Next, the area per chain can be eliminated by invoking the volume filling constraint, $\Sigma\lambda/2 = Na^3$. Insertion of these results into equation 1 and minimization with respect to λ leads to $\lambda \approx 1.03a\,\chi_{AB}^{1/6}N^{2/3}$ and $F_{lamellar} \approx 1.19(\chi_{AB}N)^{1/3}$. This prediction that the lamellar domain period scales as the two-thirds power of the copolymer molecular weight has been experimentally confirmed by Takeji Hashimoto and his colleagues.[3]

We can use our expression for the lamellar phase free energy to locate the order–disorder phase boundary. In a disordered phase, where the A and B blocks are homogeneously mixed, the free energy per chain can be approximated by the A–B contact energy alone:

$$F_{disorder}/k_BT \approx \chi_{AB}f_Af_BN = (\chi_{AB}N)/4.$$

Equating $F_{lamellar}$ to $F_{disorder}$ leads to $\chi_{AB}N = 10.4$ as the location of the order–disorder transition (ODT). This is remarkably close to a more accurate mean-field estimate of 10.5 obtained by Ludwik Leibler.[4] Thus, symmetric diblock copolymers of high molecular weight or with strongly incompatible blocks ($\chi_{AB}N > 10.5$) are predicted to be microphase separated into lamellae, whereas smaller copolymers with more compatible blocks ($\chi_{AB}N < 10.5$) are predicted to show no microphase separation.

The above simple theory, while quite restrictive in its assumptions, serves to illustrate the essential physics of microphase separation in block copolymers. The focus on a single chain highlights the mean-field character of the approach. More sophisticated mean-field theories attempt to describe nonuniform chain stretching in the microphases, arbitrary degrees of segregation strength and realistic distributions of chain end and block junction positions in the microphases. Eugene Helfand and his coworkers developed such a comprehensive theory in the mid-1970s.[5] Early applications of self-consistent mean-field theory (SCMFT) to diblock and triblock copolymers by Helfand[5] and by Jaan Noolandi and his coworkers[6] established the broad features of AB diblock and ABA triblock copolymer phase diagrams in the parameter space of the "incompatibility degree" $\chi_{AB}N$ and the one independent composition variable f_A. Leibler[4] subsequently predicted the ODT as a function of f_A and the topology of the phase diagram in the so-called weak segregation limit, where $\chi_{AB}N$ is just slightly greater than the order–disorder threshold. In the so-called strong segregation limit, $\chi_{AB}N \to \infty$, Alexander Semenov developed an alternative analytical approach (as a derivative of SCMFT) that is analogous to taking the classical limit in the path integral formulation of quantum mechanics.[7]

The most significant recent advance in the application of SCMFT to block copolymers is due to Mark Matsen and Michael Schick,[8] who identified a powerful spectral method of numerical solution that enabled them to deal with microphases of considerable three-dimensional complexity. Straightforward extensions of the theory have been developed for multicomponent systems, like alloys of block copolymers and homopolymers, and for more complex block and graft copolymer architectures, such as those shown at the bottom of figure 1. The only real limitation of the theory, besides its mean-field character, is that many basis functions are required to achieve convergence for large $\chi_{AB}N$, so calculations are practically limited to modest segregation strengths, with $\chi_{AB}N \lesssim 100$.

AB diblock configurations

Matsen and Schick's calculated phase diagram for AB diblock copolymers compares amazingly well to experimental phase diagrams on model diblock materials, as illustrated in figure 3. For $\chi_{AB}N < 10.5$, only a disordered melt is predicted. At larger values of $\chi_{AB}N$, above the ODT curve, five ordered microphase structures are predicted to have regions of thermodynamic stability. The lamellar (L) phase is stable for nearly symmetric diblocks, while a hexagonally packed cylinder (C) phase is stable for diblocks with intermediate levels of compositional asymmetry. As shown schematically in figure 2b, when $f_A > 1/2$ the smaller B blocks pack into the interiors of cylinders. This energetically preferable arrangement allows the longer A blocks to reside on the convex side of

The Gyroid Phase

First identified in 1967 by Vittorio Luzzatti and P. A. Spegt as a peculiar cubic phase in various strontium soaps, the bicontinuous gyroid (G) morphology, shown in figure 3, has emerged as a familiar state of order in soft materials. Unlike the other microphases shown in figure 3, the gyroid is one of several cubic structures characterized by domain boundaries with negative Gauss curvature (saddle surfaces). The term "gyroid" originated in 1970 with Alan Schoen,[17] a mathematician who discovered the family of triply periodic minimal surfaces that bears this name. Although complex transmission electron micrograph images of block copolymers appeared over 20 years ago, the concept of an ordered bicontinuous morphology was not recognized until the 1980s, and the G morphology was not established until 1994.[18]

Why does nature select this cubic morphology over all other complex ordered states for AB diblocks? A simple way to explore this issue is to consider the properties of the domain junctions associated with all possible bicontinuous cubic morphologies. Three-dimensional cubic networks may contain three-fold (G-surface), four-fold (D-surface) or six-fold (P-surface) connectors; the triply periodic D and P surfaces were published by Hermann A. Schwarz in 1865 and 1890, respectively. Of these, the three-fold connector contains the least curved—and hence, least crowded—microdomain interfaces, thereby best satisfying the compromise between chain stretching and interfacial tension discussed here in the text. Thus, the G phase reflects an optimized state of "frustration," a key concept in understanding the morphologies recently discovered in branched and multimonomer block copolymers, as well as oligomeric lipids, surfactants and soaps. Curiously, a survey of known organic crystal structures (Cambridge Database) yielded only 1, out of approximately 130 000 documented crystalline compounds, with the $Ia\bar{3}d$ (gyroid phase) space group symmetry. Apparently such high symmetry molecular packing favors molecules with short-range liquidlike disorder, a common ingredient of "soft materials."

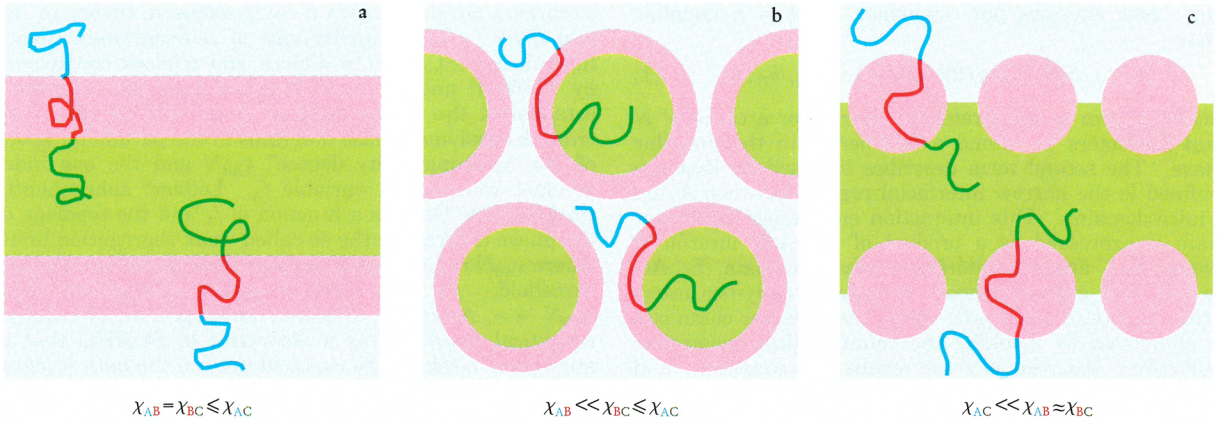

FIGURE 4. ABC TRIBLOCK MORPHOLOGY is dependent on the relative magnitude of three segment–segment interaction parameters. This point is illustrated using a compositionally symmetric ($f_A = f_B = f_C = 1/3$) model linear diblock. Microdomains are color coded as shown by the copolymer strands. **a:** With the indicated relationship of χ_{ij}, a lamellar morphology minimizes both interfacial contact energy and chain stretching. **b:** With $\chi_{AB} \ll \chi_{BC}$, a core-shell cylindrical morphology reduces the BC relative to the AB interfacial area, thereby lowering the overall free energy. **c:** A state of "frustration" occurs when $\chi_{AC} \ll \chi_{AB} \approx \chi_{BC}$. The molecular architecture requires A–B and B–C domain contacts. However, the most energetically favorable contacts are A–C. To accommodate both factors, a new, complex morphology may result. Here a "cylinder-at-the-wall" pattern is shown to illustrate this effect.

the A–B interface, which affords them more configurational entropy (or, reduces the elastic energy). With still more compositional asymmetry, the hexagonal phase gives way to a body-centered cubic spherical (S) phase. A very narrow region of close-packed spheres (CPS) separates the disordered and S phases at the composition extremes of figure 3a. Finally, Matsen and Schick predicted narrow regions of stability of a complex gyroid (G) phase close to the ODT and between the L and C phases. The G phase is a fascinating periodic bicontinuous structure that is ubiquitous in soft condensed matter systems. (See the box on page 35.)

Figure 3b shows an experimental phase diagram for a poly(isoprene-styrene) (IS) diblock copolymer melt.[9] The overall topology of the diagram is strikingly similar to the theoretical diagram in figure 3a, with a few exceptions. First, there is an overall asymmetry in figure 3b with respect to $f_A = 1/2$. It occurs partially because styrene and isoprene monomers have different sizes and shapes, so $a_A \neq a_B$ (something that was not included in the calculations summarized in figure 3a). Some of the asymmetry also results because the styrene–isoprene interactions are not accurately represented by a single χ_{IS} parameter. In other words, the free-energy cost of moving a styrene monomer from pure styrene surroundings to pure isoprene surroundings is not the same as moving an isoprene monomer from pure isoprene to pure styrene.

Besides the G phase, the experimental diagram contains small regions of a second complex phase, perforated layers (PL). According to the Matsen–Schick calculations, the PL phase is not stable in any region of the phase diagram. This discrepancy led the theory group of Shuyan Qi and Zhen-Gang Wang and the experimental group led by one of us (Frank Bates) to reexamine the PL phase.[10] Both groups concluded that the PL phase is indeed not thermodynamically stable, but is rather a long-lived transient structure with epitaxial relations to the C and L phases. Such insidious metastability is not uncommon when dealing with block copolymer melts, and this result illustrates the importance of coordinating theory and experiment. The shelf life of a product could depend on it.

A final obvious discrepancy between figures 3b and 3a concerns the region of the phase diagram near the ODT. Not only is the disordered phase stable beyond $\chi_{AB}N = 10.5$ (for $f_A = 1/2$) in the experimental diagram, but direct transitions between the disordered phase and the various ordered phases are clearly evident. In contrast, the SCMFT diagram shows the order–order lines all converging to a critical point (at $\chi_{AB}N = 10.5$ and $f_A = 1/2$), allowing only direct phase transitions between the disordered phase and the spherical (BCC and CPS) ordered phases. The explanation for this discrepancy is that composition fluctuations become important near the weakly first-order ODT curve, particularly for symmetric melts.[11]

Despite the above limitations of SCMFT, the striking overall agreement between theory and experiment for diblock copolymer melts clearly represents one of the most successful applications of mean-field theory in condensed matter physics. Matsen and Schick have gone on to apply the method to a variety of AB architectures, including ABA triblocks and $(AB)_n$ starblocks, and to explore the shifts in phase boundaries caused by conformational asymmetry. The analytical strong segregation theory developed by Semenov has also been recently extended to other architectures and used to describe complex phases such as the G phase. These analytical calculations, although more restricted in their applicability than the full numerical SCMFT, can be extremely valuable in guiding experimental design of block copolymers. For example, Scott Milner worked out the strong segregation phase diagram for A_2B graft copolymers with two A arms and one B arm (diagrammed in figure 1).[12] As shown in figure 2c, the crowding of the extra A arms in the A microdomains strongly drives interfacial curvature away from A. This architectural asymmetry can be much more effective at shifting phase boundaries between ordered microphases than the weaker conformational (monomer size and shape) asymmetry. Milner's phase diagram for such graft copolymers is highly asymmetric in f_A and this asymmetry has been borne out by recent experiments on model A_2B materials.

And then there were three

Even more exciting possibilities for self-assembly are created by formulating block copolymers with three or more distinct types of blocks. As illustrated in figure 1 for

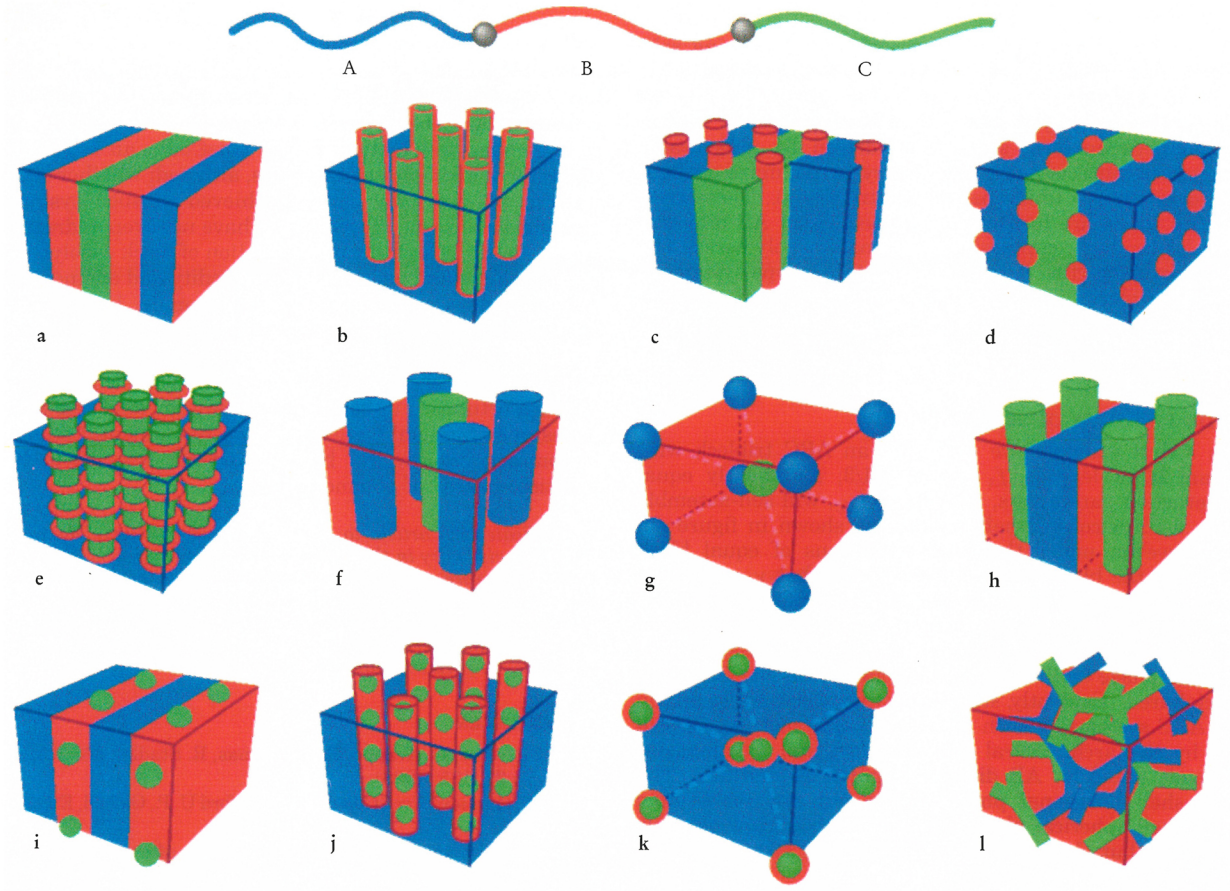

FIGURE 5. MORPHOLOGIES FOR LINEAR ABC triblock copolymers. A combination of block sequence (ABC, ACB, BAC), composition and block molecular weights provides an enormous parameter space for the creation of new morphologies. Microdomains are colored as shown by the copolymer strand at the top, with monomer types A, B and C confined to regions colored blue, red and green, respectively. (Adapted from Zheng and Wang in ref. 13.)

"three color" ABC block copolymers, a large number of architectures can be synthetically accessed, including both linear and branched arrangements. Block sequence plays an important role in this class of materials, and so the morphologies and phase transitions that can be accessed in ABC triblocks may be quite different from those in BAC or ACB triblocks. Associated with this increase in architectural complexity is a dramatic increase in the complexity and number of self-assembled microphase structures. Although only four (equilibrium) microphase structures have been observed in AB and ABA systems (the L, G, C and S phases shown in figure 3), more than a dozen have already been identified in the (rather limited) experiments on ABC systems to date.

As one might anticipate, the parameter space greatly expands as one moves from AB diblocks to ABC block systems. Although $\chi_{AB}N$ and f_A are sufficient to locate a point in the mean-field phase diagram for AB diblocks, three interaction parameters (χ_{AB}, χ_{AC}, χ_{BC}) and two independent composition variables (such as f_A and f_B) are the minimum required to specify the phase state of ABC triblocks. Even more architectural parameters are required to differentiate phase diagrams of ABC systems with different block sequence or chain architecture.

This dramatic expansion of parameter space poses both experimental and theoretical challenges. Experimentally, the preparation of a sample consists of a laborious sequence of synthesis, isolation and characterization steps. Each change in composition, molecular weight or architecture requires that these steps be repeated. Although combinatorial chemistry techniques hold some promise for massively parallel synthesis in the future, such techniques have not yet had an impact on the exploration of ABC block copolymer phase behavior. Another experimental challenge is that the equilibration of ABC systems can be exceedingly difficult. Long-lived metastable states are readily produced by solvent casting, precipitation or thermal quenching. Such metastable states may have desirable properties, but theoretical prediction of their existence or lifetime is very difficult. Great care must be taken to achieve morphological states that are independent of sample preparation procedures.

On the theoretical side, there are comparable challenges because SCMFT calculations are numerically intensive. A great deal of computational effort is involved in mapping phase diagrams in a large parameter space with numerous competing microphase structures. A limitation of current theoretical techniques is that they proceed by assuming a periodic structure, computing its free energy and then comparing that free energy to the free energies of other candidate structures. Such calculations run the risk of overlooking complex three-dimensional microphases that have not been previously identified. Close interaction between experiment and theory is clearly required in this challenging area of materials science.

Despite the challenges, quite a bit of progress has

been made in understanding the physics governing self-assembly in the simplest of ABC systems—linear ABC triblock copolymer melts. As in AB diblock melts, the physics in these systems fundamentally reflects a competition between local segregation driven by unfavorable monomer contacts and the tendency to maximize configurational entropy (minimize chain stretching). These competing forces are further constrained, as in AB diblocks, by the limited compressibility of molten polymers. The primary distinction between ABC and AB type systems is that the blocks in ABC systems can be driven to adopt more complex configurations due to the competing constraints—termed "frustration"—of the three distinct binary interactions.

The richness of self-assembly

As a first example, we note that an ABC triblock with equal block lengths, $f_A = f_B = f_C = 1/3$, and nearly equal interaction parameters, $\chi_{AB} \approx \chi_{AC} \approx \chi_{BC}$, will self-assemble into a three-color lamellar phase as shown in figure 4a. If, however, under the same conditions of equal block lengths, the blocks are sequenced such that $\chi_{AB} \ll \chi_{BC}$, a spontaneous curvature of the AB and BC interfaces is induced. As illustrated in figure 4b, the melt is driven by this interaction asymmetry to adopt a core-shell hexagonal phase (with C cores) that minimizes the BC interfacial area. Evidently, structural transitions can be driven in ABC systems by such interaction asymmetries, as well as by the architectural and compositional asymmetries already noted for AB diblocks (figures 2b and 2c). The core-shell hexagonal phase (figure 5b) and the related core-shell spherical phase (figure 5k) have been not only observed but also justified on the basis of strong-segregation theoretical calculations.[13]

Another type of frustration in ABC triblock systems leads to the unusual microstructures in figure 5, where red B blocks decorate the AC interfaces in the form of cylinders (5c), spheres (5d) and rings (5e). These structures were discovered by Stadler and his colleagues. Here, $\chi_{AB} \approx \chi_{BC} \gg \chi_{AC}$, so that the middle B block is strongly disliked by both end blocks. Rather than provide a continuous B layer separating A and C, as in the core-shell structures 5b and 5k, under such conditions the B layer becomes discontinuous, allowing for increased AC contacts. As a result, for small values of f_B, one of the structures 5c, 5d or 5e is favored, depending on the proportions of A and C. As f_B is increased, the B microdomains are forced to become continuous and the "cylinders-at-the-wall" structure 5c ultimately transforms to the lamellar phase 5a. (The knitting pattern shown on the cover is a product of this type of frustration.)

A third class of structures, also shown in figure 5, has been observed in nearly "symmetric" systems where $\chi_{AB} \approx \chi_{BC} < \chi_{AC}$ and $f_A \approx f_C$. A beautiful experimental study of such a system was carried out by Yushu Matsushita and his coworkers.[14] On increasing the B content, f_B, they reported the following sequence of morphologies: 5a, 5l, 5f and 5g. Structures 5f (tetragonal cylinders) and 5g have staggered lattices of A and C aggregates that are arranged to eliminate AC contacts, yet minimize extension of the B blocks. Structure 5l is a tricontinuous G morphology that is composed of independent A and C networks. Recent SCMFT calculations by Matsen[15] indicate that this double gyroid is actually an equilibrium structure.

Although the above examples serve to illustrate the richness of self-assembly behavior exhibited by block copolymer systems, they also indicate that knowledge and exploitation of such systems remains quite limited. In particular, only small regions of the full parameter space accessible in ABC systems have been examined to date, and we are unaware of any significant commercial applications of ABC block copolymers. Copolymers with four or five chemically distinct blocks must offer an incredible diversity of microphase structures, although whether equilibrium self-assembly can be achieved in such systems remains to be seen. Moreover, we have not even addressed the industrially significant application of block copolymers as emulsifiers and additives in commodity and engineering polymer alloys. Recent work, for example, has demonstrated that AB and possibly ABC block copolymers can be rationally designed to stabilize co-continuous, "polymeric microemulsion" phases in ternary polymer blends.[16] Vast opportunities undoubtedly remain for applying principles of self-assembly gleaned from fundamental studies of complex, "multicolor" block copolymer systems to the practical design of polymer alloys.

We dedicate this article to our friend and colleague Reimund Stadler, a visionary in the field of block copolymers, who died last June. This work was supported by the National Science Foundation under Award Number DMR-9870785 (GHF) and DMR-9405101 (FSB). We are grateful to Ned Thomas for providing the cover figure and Terri Shefelbine for stimulating discussions and assistance in preparing the illustrations.

References

1. U. Breiner, U. Krappe, E. L. Thomas, R. Stadler, *Macromolecules* **31**, 135 (1998).
2. I. W. Hamley, *Block Copolymers*, Oxford U. P., Oxford, England (1999).
3. T. Hashimoto, M. Shibayama, H. Kawai, *Macromolecules* **13**, 1237 (1980).
4. L. Leibler, *Macromolecules* **13**, 1602 (1980).
5. E. Helfand, Z. R. Wasserman, *Macromolecules* **9**, 879 (1976); **11**, 960 (1978); **13**, 994 (1980).
6. J. Noolandi, K. M. Hong, *Ferroelectrics* **30**, 117 (1980). K. M. Hong, J. Noolandi, *Macromolecules* **14**, 727 (1981). M. D. Whitmore, J. Noolandi, *J. Chem. Phys.* **93**, 2946 (1990).
7. A. N. Semenov, *Sov. Phys. JETP* **61**, 733 (1985).
8. M. W. Matsen, M. Schick, *Phys. Rev. Lett.* **72**, 2660 (1994); *Macromolecules* **27**, 6761 (1994); **27**, 7157 (1994). M. W. Matsen, F. S. Bates, *Macromolecules*, **29**, 1091 (1996).
9. A. K. Khandpur, S. Förster, F. S. Bates, I. W. Hamley, A. J. Ryan, W. Bras, K. Almdal, K. Mortensen, *Macromolecules* **28**, 8796 (1995).
10. S. Qi, Z.-G. Wang, *Phys. Rev. E* **55**, 1682 (1997); D. A. Hajduk, H. Takenouchi, M. A. Hillmyer, F. S. Bates, M. E. Vigild, K. Almdal, *Macromolecules* **30**, 3788 (1997).
11. G. H. Fredrickson, E. Helfand, *J. Chem. Phys.* **87**, 697 (1987). F. S. Bates, J. H. Rosedale, G. H. Fredrickson, C. Glinka, *Phys. Rev. Lett.* **61**, 2229 (1988).
12. S. T. Milner, *Macromolecules* **27**, 2333 (1994).
13. R. Stadler, C. Aushra, J. Beckmann, U. Krappe, I. Voigt-Martin, L. Leibler, *Macromolecules* **28**, 3080 (1995). W. Zheng, Z.-G. Wang, *Macromolecules* **28**, 7215 (1995).
14. Y. Matsushita, J. Suzuki, M. Seki, *Physica B* **248**, 238 (1998). Y. Mogi, M. Nomura, H. Kotsuje, K. Ohnishi, Y. Matsushita, I. Noda, *Macromolecules* **27**, 6755 (1994).
15. M. W. Matsen, *J. Chem. Phys.* **108**, 785 (1998).
16. F. S. Bates, W. W. Maurer, P. M. Lipic, M. A. Hillmyer, K. Almdal, K. Mortensen, G. H. Fredrickson, T. P. Lodge, *Phys. Rev. Lett.* **79**, 849 (1997). G. H. Fredrickson, F. S. Bates, *Eur. Phys. J. B.* **1**, 71 (1998).
17. A. Schoen, *NASA TechNote* TN D-5541 (1970).
18. D. A. Hajduk, P. E. Harper, S. M. Gruner, C. Honeker, G. Kim, E. L. Thomas, L. J. Fetters, *Macromolecules* **27**, 4063 (1994). M. F. Schulz, F. S. Bates, K. Almdal, K. Mortensen, *Phys. Rev. Lett.* **73**, 86 (1994). ■